Modeling of Conductor-Loaded Resonators and Filters in Rectangular Enclosures

Chi Wang, Hui-Wen Yao, *Senior Member IEEE,* and Kawthar A. Zaki, *Fellow, IEEE*

***Abstract*—Full-wave modeling of conductor-loaded resonators in rectangular enclosures and the associated coupling structure is presented. The modeling yields generalized scattering matrices of the cylindrical conductor-loaded resonators in rectangular waveguides. By applying short and open conditions and cascading procedure, resonant frequencies, field distributions of the resonator, and coupling coefficients between two cavities through an iris are obtained. The computed results are compared with the measured data and both are in good agreement. A four- and an eight-pole dual-mode elliptic-function filter were designed, constructed, and tested. Measured frequency responses of the filters verify the theory.**

I. Introduction

HIGH-PERFORMANCE small-size microwave resonators and filters are finding increasing applications in modern communication systems. Dual-mode technique and dielectric-loaded resonators have been widely used in many applications [1]–[4]. Recently, a new type of resonator (i.e., dual-mode conductor-loaded resonator) was introduced [14], [15]. The resonator has much lower cost, weight, and better spurious performance than the dielectric-loaded resonators. The unloaded Q of the new-type resonator is less than that of the dielectric-loaded resonator, but is much higher than that of the coaxial and combline resonators. The new type of resonators and filters has potential in many practical applications, such as personal-communication system (PCS) and personal-communication network (PCN) base-station filters. As for the case of the conventional cylindrical dual-mode filter structure, it is difficult to support the resonator in the cavity when the number of cavities is more than two. The proposed structure, shown in Fig. 1 (i.e., conductor-loaded resonator with dielectric support mounted in a rectangular enclosure), can avoid the above difficulty and increase the mechanical stability of the resonator [10].

Full-wave modeling of cylindrical objects in a rectangular waveguide is not an easy task because the problem involves two kinds of coordinate systems. Although purely numerical methods such as the finite-element method can be applied to solve the problem, the accuracy and the efficiency of the methods usually make them not suitable for the narrow-bandwidth filter design. The accuracy of the results by the point-matching method [8] and the moment method [9] is also not as good as the mode-matching method. However, the integrals in the inner products of the mode-matching method can not be directly analytically evaluated. By expanding the fields in the rectangular waveguide into cylindrical wave functions using the Bessel–Fourier series, the integration for each term of the series can be obtained analytically [11]–[13]. Several kinds of cylindrical objects in rectangular waveguide have been successfully solved. Reliable and accurate results were obtained by the method. Furthermore, the generalized scattering matrices of the rectangular waveguide to cylindrical system discontinuity can be treated as a key building block so that more complicated problems can be solved.

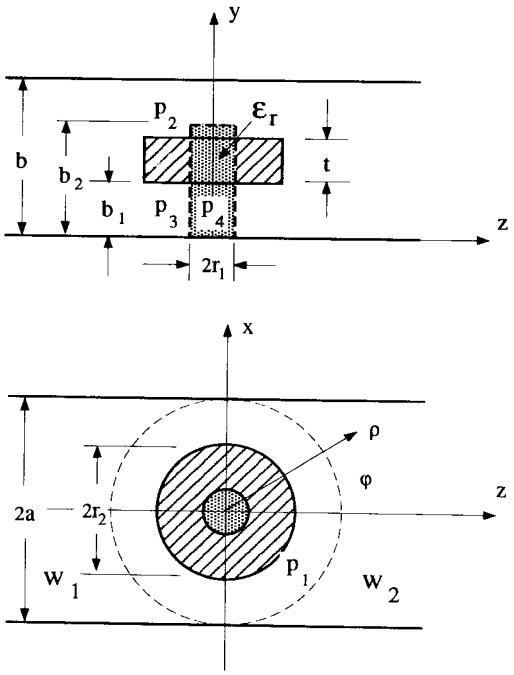

Fig. 1. Configuration of a generalized conductor-loaded resonator with support in a rectangular waveguide.

In this paper, the discontinuity in the cylindrical region (i.e., the conductor-loaded resonator), is modeled by the radial mode-matching method and the approach using the Bessel–Fourier series as [11]–[13] is used to solve the cylindrical region to rectangular-waveguide discontinuity. As a result, the generalized scattering matrices of the conductor-loaded resonator in rectangular waveguide are obtained. By applying a short condition at both ends of the cavity, resonant frequencies and field distributions of the resonator can be obtained. Using the cascading procedure [5], coupling coefficients between two cavities through an iris are calculated.

Manuscript received March 31, 1997; revised August 18, 1997.

C. Wang and K. A. Zaki are with the Department of Electrical Engineering, University of Maryland, College Park, MD 20742 USA.

H.-W. Yao is with Space Optical Group, Orbital Sciences Corporation, Germantown, MD 20374 USA.

Publisher Item Identifier S 0018-9480(97)08359-2.

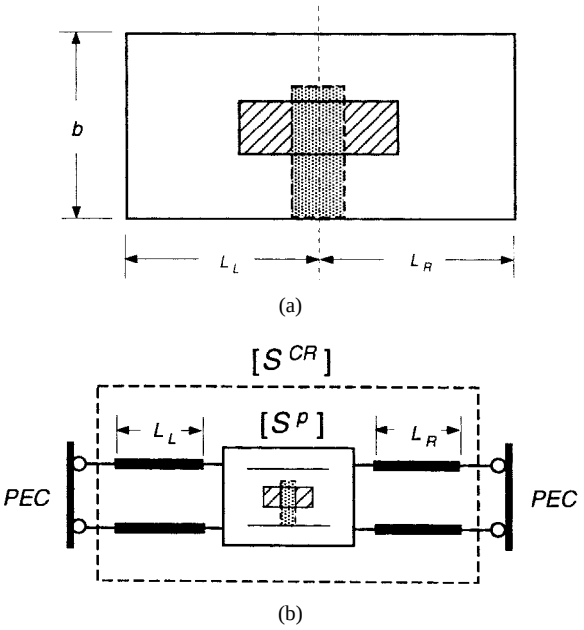

Fig. 2. (a) Configuration of a conductor-loaded rectangular cavity. (b) Network representation of the cavity.

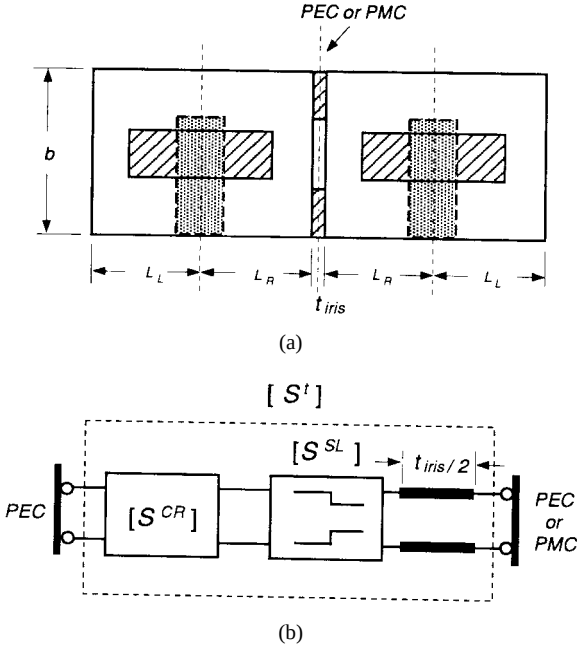

Fig. 3. (a) Coupling structure between two conductor-loaded rectangular cavities through an iris. (b) Network representation of the structure.

The computed results are compared with the measured data and are shown to be in good agreement. A four- and an eight-pole dual-mode elliptic-function filter using the proposed structure were designed, constructed, and tested. Measured frequency responses of the filters verify the theory.

II. Analysis

The configuration of a conductor-loaded resonator in a rectangular waveguide under consideration is shown in Fig. 1. A conductor ring of thickness t, inner radius r_1, and outer radius r_2, supported by a dielectric rod of height b_2, is mounted in a rectangular waveguide. A conductor-loaded cavity can be viewed as a conductor-loaded waveguide shorted at both ends, as shown in Fig. 2(a). The coupling structure consisting of two conductor-loaded cavities with a rectangular iris in their common wall is shown in Fig. 3(a). The analysis of the structure can be obtained by cascading the generalized scattering matrices of the different elements. By solving for the generalized scattering matrix of the conductor-loaded rectangular waveguide, one can find the solutions of both the conductor-loaded cavity and its coupling structure.

A. Scattering Parameters of the Conductor-Loaded Resonator in a Rectangular Waveguide

The structure of Fig. 1 is divided into two main regions: the cylindrical region, defined as $\rho \le a$, and the rectangular-waveguide region, defined as $\rho > a$, $|x| < a$. The cylindrical region is further divided into three one-layer regions and one two-layer region along the radial direction, while the waveguide region is divided into left region w_1 and right region w_2. Modeling of the structure reduces to finding the generalized scattering matrices for the two key building blocks: cylindrical discontinuities, which are obtained using radial mode matching, and the rectangular waveguide to cylindrical region discontinuity, which is obtained by mode-matching techniques. For this type of discontinuity, the mutual inner-product integrations are analytically computed through the Bessel–Fourier series. The analysis is similar to [12] and is briefly summarized below.

1) Discontinuity in Cylindrical Regions: The fields in the cylindrical regions are expanded as the summation of the two parallel-plate waveguide's eigenfields in each region in cylindrical coordinates (ρ, ϕ, y). The transverse fields with respect to the ρ direction can be expressed as

$$\vec{E}_t^p(\rho,\phi,y) = \sum_n \sum_{q=e,h} \sum_j \left\{ C_{nj}^{pq} \mathcal{B}_{CEnj}^{pq}(\rho) + D_{nj}^{pq} \mathcal{B}_{DEnj}^{pq}(\rho) \right\} \cdot \vec{e}_{ctnj}^{pq}(\rho,\phi,y) \quad (1a)$$

$$\vec{H}_t^p(\rho,\phi,y) = \sum_n \sum_{q=e,h} \sum_j \left\{ C_{nj}^{pq} \mathcal{B}_{CHnj}^{pq}(\rho) + D_{nj}^{pq} \mathcal{B}_{DHnj}^{pq}(\rho) \right\} \cdot \vec{h}_{ctnj}^{pq}(\rho,\phi,y) \quad (1b)$$

$$p = I, II, III, IV$$

where $\mathcal{B}_{CEj}^{pq}$ and $\mathcal{B}_{CHj}^{pq}$ are the first-kind Bessel functions J_n or associated Bessel functions I_n, and their derivatives of TE_y ($q = h$) and TM_y ($q = e$) modes. $\mathcal{B}_{DEj}^{pq}$ and $\mathcal{B}_{DHj}^{pq}$ are the second-kind Bessel functions Y_n or associated Bessel functions K_n, and their derivatives [15]. $\vec{e}_{ctnj}^{pq}$, $\vec{h}_{ctnj}^{pq}$ are the transverse eigenfields of TE_y and TM_y modes in the two parallel-plane waveguide bounded in the y-direction, and are given in the Appendix.

By forcing the tangential electric and magnetic fields of the cylindrical regions to be continuous at $\rho = r_1$ and $\rho = r_2$, and taking proper inner products, a matrix relating the field coefficients in region I can finally be obtained as

$$\left[[M_C^I][M_D^I] \right] \begin{bmatrix} C^I \\ D^I \end{bmatrix} = 0 \quad (2)$$

where $[M_C^I]$ and $[M_D^I]$ are highly sparse matrices containing the block matrices corresponding to the inner products of the eigenmodes with each ϕ variation at the diagonals of $[M_C^I]$ and $[M_D^I]$.

2) Rectangular Waveguide to Cylindrical Region Discontinuity: The fields in waveguide regions are related to the fields in cylindrical region I by the boundary condition at the artificial boundary $\rho = a$. The tangential electromagnetic fields in the waveguide regions at the artificial boundary can be expressed as

$$\vec{E}_{wt}^{i}(\rho,\phi,y) = \sum_{q=e,h}\sum_{m}\sum_{j}\Big\{A_{mj}^{iq}\exp^{\pm\gamma_{mj}^{q}\rho\cos\phi} + B_{mj}^{iq}\exp^{\mp\gamma_{mj}^{q}\rho\cos\phi}\Big\} \cdot \vec{e}_{wtmj}^{iq}(\rho,\phi,y) \tag{3a}$$

$$\vec{H}_{wt}^{i}(\rho,\phi,y) = \sum_{q=e,h}\sum_{m}\sum_{j}\Big\{A_{mj}^{iq}\exp^{\pm\gamma_{mj}^{q}\rho\cos\phi} - B_{mj}^{iq}\exp^{\mp\gamma_{mj}^{q}\rho\cos\phi}\Big\} \cdot \vec{h}_{wtmj}^{iq}(\rho,\phi,y) \tag{3b}$$

$$\begin{aligned}\vec{e}_{wtmj}^{iq}(\rho,\phi,y) &= -\hat{\rho}\times\left(\hat{\rho}\times\vec{e}_{wmj}^{iq}(x,y)|_{x^2+z^2=a^2}\right)\\ &= \hat{y}e_{wymj}^{iq}(x,y) + \hat{\phi}\Big[e_{wxmj}^{iq}(x,y)\cos\phi \mp e_{wzmj}^{iq}(x,y)\sin\phi\Big]\end{aligned} \tag{4a}$$

$$\begin{aligned}\vec{h}_{wtmj}^{iq}(\rho,\phi,y) &= -\hat{\rho}\times\left(\hat{\rho}\times\vec{h}_{wmj}^{iq}(x,y)|_{x^2+z^2=a^2}\right)\\ &= \pm\hat{y}h_{wymj}^{iq}(x,y) + \hat{\phi}\Big[h_{wxmj}^{iq}(x,y)\cos\phi \mp h_{wzmj}^{iq}(x,y)\sin\phi\Big]\end{aligned} \tag{4b}$$

$$i = w_1, w_2$$

where the upper part of the sign in the exponential term applies for the fields in region w_1, and the lower sign applies for the fields in region w_2. $\vec{e}_{wmj}^{iq}$ and $\vec{h}_{wmj}^{iq}$ are eigenmode fields of TE_z ($q = h$) and TM_z ($q = e$) modes in the rectangular waveguide. $\vec{e}_{wtmj}^{iq}$ and $\vec{h}_{wtmj}^{iq}$ are the tangential fields of $\vec{e}_{wmj}^{iq}$ and $\vec{h}_{wmj}^{iq}$ at the interface of the artificial boundary $\rho = a$.

Matching the tangential electromagnetic fields of the two waveguide regions and cylindrical region I on the imaginary boundary $\rho = a$, taking the cross inner products, and using the method described in [12] and [13], a matrix equation relating the field coefficients of the incident and reflected waves in the waveguide regions w_1 and w_2 to the coefficients of cylindrical region I can be obtained as follows:

$$\begin{bmatrix}C^I\\ D^I\end{bmatrix} = [M_A]\begin{bmatrix}A^{w_1}\\ A^{w_2}\end{bmatrix} + [M_B]\begin{bmatrix}B^{w_1}\\ B^{w_2}\end{bmatrix}. \tag{5}$$

From (2) and (5), the desired generalized scattering matrix of the conductor-loaded resonator in a rectangular waveguide can be obtained as follows:

$$\begin{bmatrix}B^{w_1}\\ B^{w_2}\end{bmatrix} = \begin{bmatrix}[S_{11}^P] & [S_{12}^P]\\ [S_{21}^P] & [S_{22}^P]\end{bmatrix}\begin{bmatrix}A^{w_1}\\ A^{w_2}\end{bmatrix} = [S^P]\begin{bmatrix}A^{w_1}\\ A^{w_2}\end{bmatrix}. \tag{6}$$

B. Conductor-Loaded Rectangular Cavity

The conductor-loaded rectangular cavity can be modeled using the generalized scattering matrix of the conductor-loaded resonator. The reference planes of the two-port network are moved distances L_L and L_R from the center of the resonator. Short circuits are placed at these ports, as shown in Fig. 2. Then the characteristic equation for the resonant frequency of the cavity can be obtained as follows:

$$\det\left\{[S^{CR}] + [I]\right\} = 0. \tag{7}$$

The zeros of the determinant of the matrix in (7) are the resonant frequencies of the cavity. Solving matrix equations (6) and (7) at each resonant frequency gives the field coefficients of the resonant mode in the waveguide region. All the other field coefficients in the cylindrical regions can be calculated from the continuity equation at the boundaries. The field distribution of the resonant mode can then be computed.

C. Slot Coupling Between Two Identical Cavities

To compute the coupling between two identical cavities through an iris, properties of the symmetrical network can be used to simplify the computation, as shown in Fig. 3. By applying a perfect electric conductor (PEC) and a perfect magnetic conductor (PMC) boundary condition at the symmetrical plane, the coupling structure can be modeled as a conductor-loaded cavity connected with an evanescent-mode waveguide, whose length is half the iris thickness. The generalized scattering matrices of the two-port structure $[S^t]$ can then be obtained using the cascading procedure, as shown in Fig. 3(b). Applying the boundary conditions at both ends of the structure, the following characteristic equations for the structure are obtained:

$$\det\begin{bmatrix}[S_{11}^t] + [I] & [S_{12}^t]\\ [S_{21}^t] & [S_{22}^t] \pm [I]\end{bmatrix} = 0 \tag{8}$$

where $+$ is used for the PEC wall at the symmetric plane, which gives resonant frequency f_e, and $-$ for the PMC wall, which gives resonant frequency f_m.

The coupling coefficient can be computed from the two resonant frequencies f_e and f_m as [6]

$$k = \frac{M}{L} = \frac{f_e^2 - f_m^2}{f_e^2 + f_m^2}. \tag{9}$$

III. Results

A computer program has been developed to compute the resonant frequencies, field distributions, and coupling coefficients of the conductor-loaded rectangular cavities. The field distributions of the HE_{11} mode of a cavity are shown in Fig. 4. The fields satisfy the boundary conditions at the interface of each region, thus ensuring the correctness of the results. Both electric- and magnetic-field distributions are shown at various cross sections of the resonator. The field distributions of the orthogonal mode with the PEC at $x = 0$ plane have the same shape, but are rotated through a 90° angle.

The resonant frequencies of a conductor-loaded rectangular cavity for different modes are computed and compared with

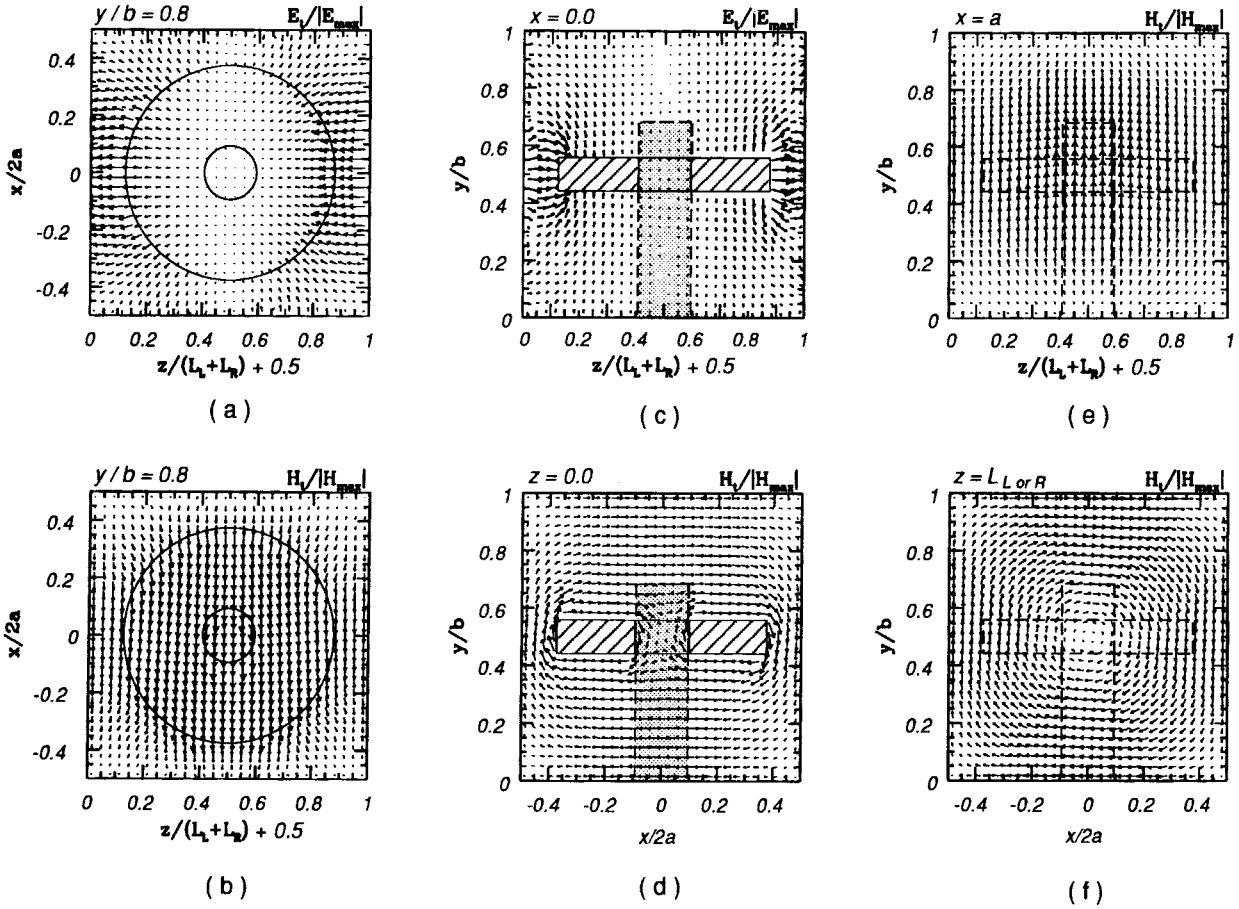

Fig. 4. Field distributions of a conductor-loaded rectangular cavity with $2a = 1.2$ in, $b = 1.0$ in, $r_1 = 0.0$ in, $r_2 = 0.45$ in, $t = 0.1$ in, $b_1 = 0.45$ in. (a) Electric-field distribution at $y = 0.8$-in plane with PMC at $x = 0$ plane. (b) Magnetic-field distribution at $y = 0.8$-in plane with PMC at $x = 0$ plane. (c) Magnetic-field distribution at $z = \pm 0.6$-in plane with PMC at $x = 0$ plane. (d) Magnetic field distribution at $z = \pm 0.6$-in plane with PEC at $x = 0$ plane.

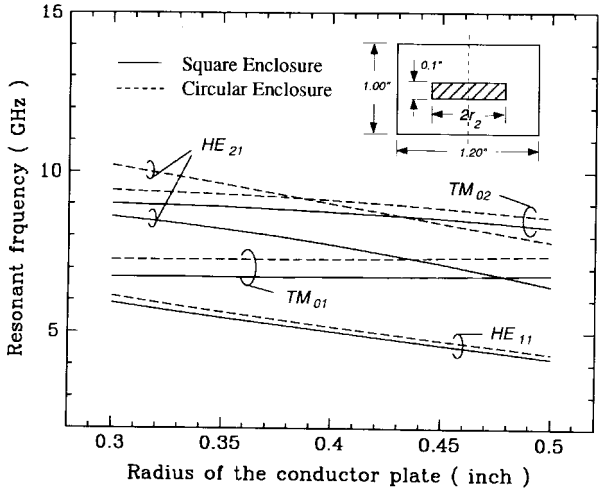

Fig. 5. Mode chart of a conductor-loaded rectangular cavity with $2a = 1.2$ in, $b = 1.0$ in, $r_1 = 0.0$, $t = 0.1$ in, $b_1 = 0.45$ in, versus radius r_2.

TABLE I
COMPARISON OF COMPUTED AND MEASURED RESONANT FREQUENCIES IN GHz WITH $2a = 1.2$ in, $b = 1.0$ in, $r_1 = 0$, $r_2 = 0.45$ in, $L_L = L_R = 0.6$ in, $\epsilon_r = 1.02$

	HE_{11}	TM_{01}	HE_{21}	TM_{02}	HE_{12}
computed	4.555	6.672	7.066	8.461	10.631
measured	4.549	6.631	7.082	8.478	10.575

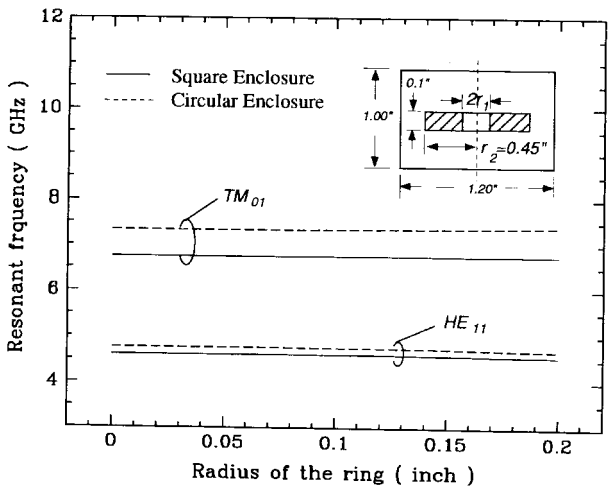

Fig. 6. Effect of ring of a conductor-loaded rectangular cavity with $2a = 1.2$ in, $b = 1.0$ in, $r_2 = 0.45$ in, $t = 0.1$ in, $b_1 = 0.45$ in, on resonant frequencies of the first two modes.

the measured results in Table I, and both results are in good agreement. Fig. 5 shows the resonant frequencies of the first five modes in a cavity with a solid conductor plate versus the radius of the plate. The resonant frequencies of the rectangular cavity are also compared with that of the cylindrical enclosure of $\rho = a$. It is seen that the resonant frequency

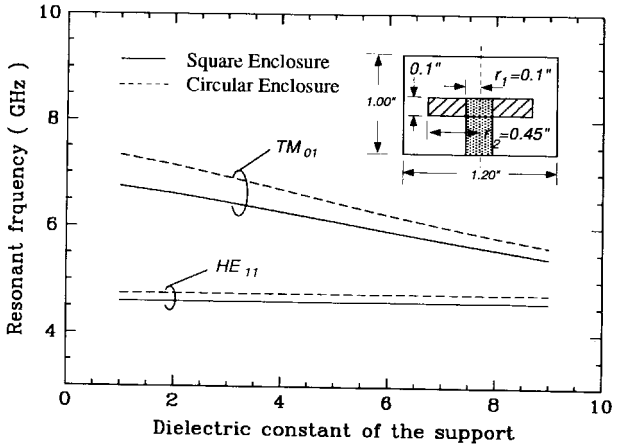

Fig. 7. Effect of the dielectric constant of the support on the resonant frequencies of the first two modes of a conductor-loaded rectangular cavity with $2a = 1.2$ in, $b = 1.0$ in, $r_1 = 0.1$ in, $r_2 = 0.45$ in, $t = 0.1$ in, $b_1 = 0.45$ in.

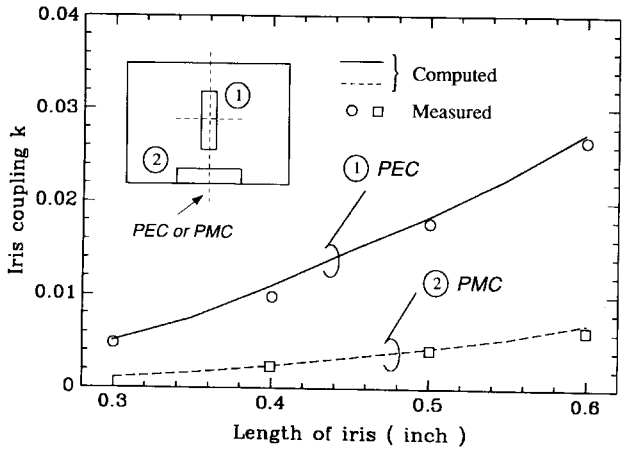

Fig. 8. Coupling coefficients between two identical conductor-loaded rectangular cavities with $2a = 1.2$ in, $b = 1.0$ in, $r_1 = 0.0$, $r_2 = 0.45$ in, $t = 0.1$ in, $b_1 = 0.45$ in, versus the length of the iris of 0.1-in width.

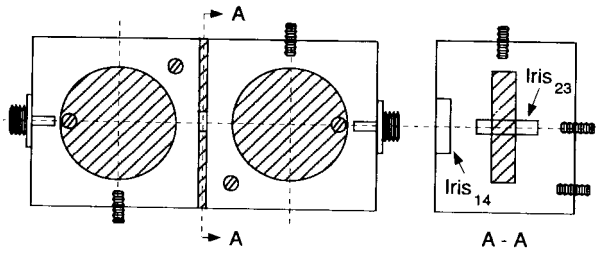

Fig. 9. Configuration of the test dual-mode four-pole elliptic-function filter.

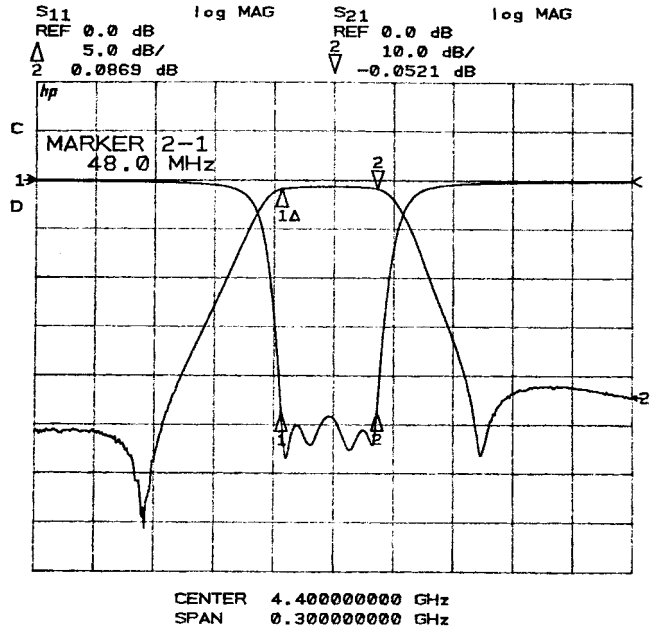

Fig. 10. Measured frequency responses of the test dual-mode four-pole elliptic-function filter.

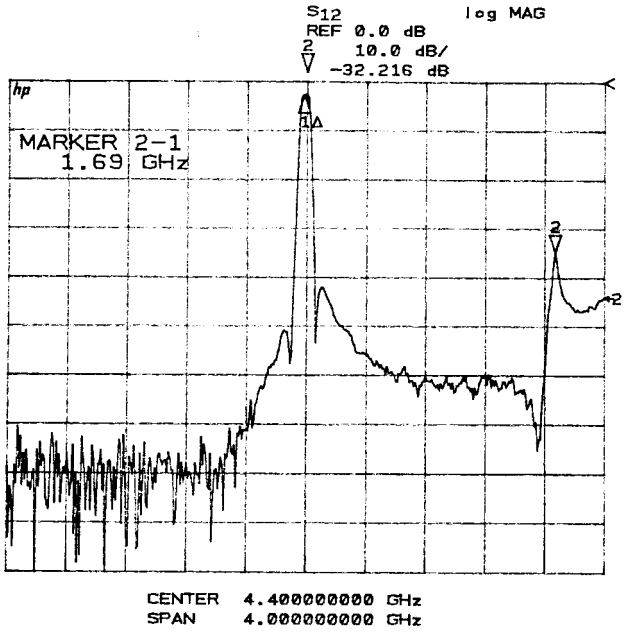

Fig. 11. Wide-band frequency response of the test dual-mode four-pole elliptic-function filter.

of the rectangular enclosure is lower than that of cylindrical enclosure, especially for the HE_{21} mode, but has the same trends for both kinds of enclosures. Fig. 6 shows the resonant frequencies of the cavity versus the radius of the hole in the loading element. The hole of the conductor plate does not have a strong effect on the resonant frequency of the first and second modes. Fig. 7 shows the resonant frequencies of the cavity versus the dielectric constant of the support. It is seen that the dielectric constant of the support has a strong effect on the resonant frequency of the second mode (TM_{01}) of the cavity.

The coupling coefficients between two identical conductor-loaded rectangular cavities through an iris with PEC and PMC boundary conditions at $x = 0$ plane are also computed and compared with the measured results (see Fig. 8). It is shown that strong coupling can be achieved with PEC at $x = 0$ plane. Both calculated and measured couplings are in good agreement.

As an application of the modeling, a four-pole elliptic-function filter with center frequency of 4.40 GHz and bandwidth of 48 MHz is designed, constructed, and tested. The normalized input/output resistances and coupling matrix ele-

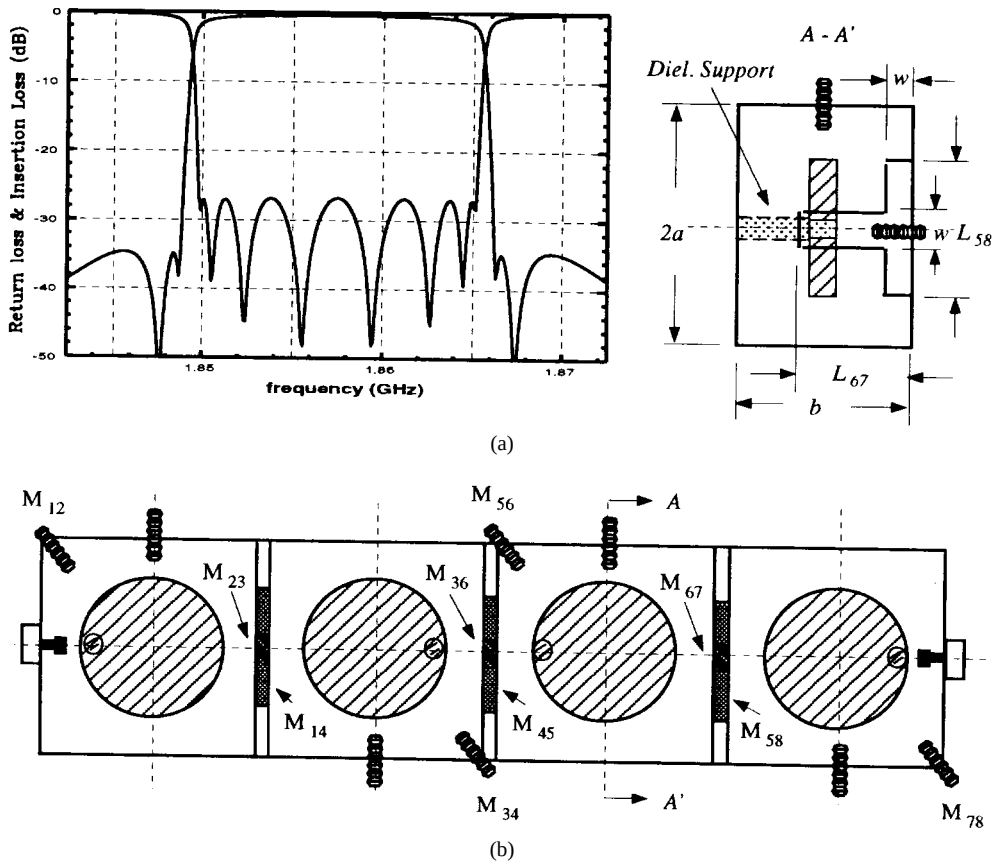

Fig. 12. (a) Theoretical frequency responses of the eight-pole filter. (b) Configuration of the designed filter.

ments of the filter as obtained from synthesis are as follows:

$$M = \begin{bmatrix} 0 & 0.9799 & 0 & -0.1095 \\ 0.9799 & 0 & 0.7875 & 0 \\ 0 & 0.7875 & 0 & 0.9799 \\ -0.1095 & 0 & 0.9799 & 0 \end{bmatrix}$$
$$R_A = R_B = 1.2535. \tag{10}$$

The configuration of the filter is shown in Fig. 9. The tuning screws on the top and at the side of the conductors oriented at 0° and 90° to the normal field polarization in each resonator are used for resonant frequency tuning. The tuning screws on the top of the conductors oriented at 45° are used for obtaining the coupling M_{12} and M_{34}. The vertical iris is used to obtain M_{23} and the horizontal iris is used to achieve the negative coupling M_{14}. The relative position of the 45° tuning screws determines the sign of coupling M_{14}. The measured frequency responses of the test filter are shown in Fig. 10. It is seen that the measured responses are in agreement with the theoretical responses. Fig. 11 is the wide-band frequency response of the four-pole filter. The first spurious response which is coupled by the vertical iris from TM_{01} mode is 1.69 GHz higher than the center frequency of the filter.

Finally, an eight-pole elliptic-function filter for PCS base-station application with center frequency of 1.8575 GHz, and bandwidth of 15.5 MHz was designed and constructed. Fig. 12 shows the theoretical frequency responses and the configuration of the filter. The conductor-loaded resonators are supported by low dielectric-constant material. All the irises are opened at one side of the filter to simplify the structure.

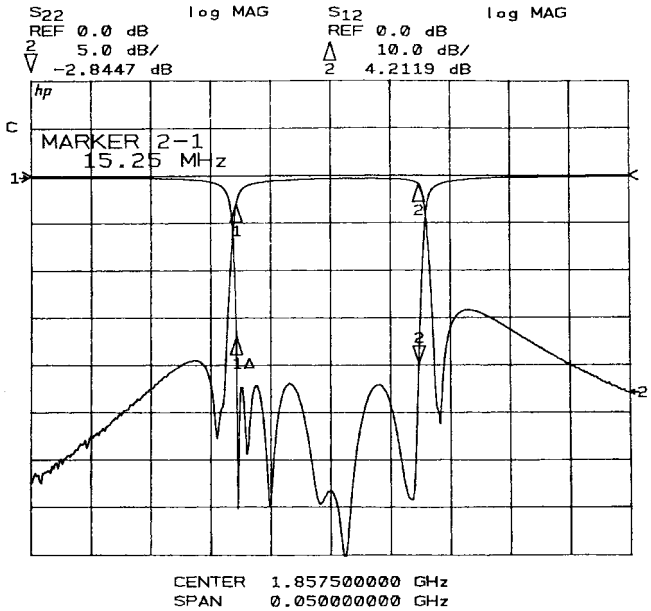

Fig. 13. Measured frequency responses of the eight-pole filter.

Fig. 13 shows the measured frequency responses of the filter. The insertion loss of the filter at the center frequency is 0.70 dB. The corresponding realized Q is larger than 6000.

IV. Conclusion

Conductor-loaded resonators in a rectangular enclosure and their coupling structures are modeled by a rigorous mode-

matching method. The computed resonant frequencies and coupling coefficients of the cavity are compared with the measured data and shown to be in good agreement. A four- and an eight-pole dual-mode elliptic-function filter were designed, constructed, and tested. Measured frequency responses of the filters verify the theory. Dual-mode conductor-loaded resonator filters have better out-of-band spurious response compared to the corresponding dielectric-loaded resonators.

APPENDIX

This appendix gives the expressions for the transverse eigenfields of two parallel-plane waveguides $\vec{e}^{pq}_{ctnj}$ and $\vec{h}^{pq}_{ctnj}$.

For TE_y mode:

$$\vec{e}^{ph}_{ctnj}(\rho,\phi,y) = \hat{\phi}\frac{1}{\xi_j^{ph^2}}\Phi^h_n(\phi)h^{ph}_{yj}(k_j^{ph},y) \tag{A1}$$

$$j\omega\mu\vec{h}^{ph}_{ctnj}(\rho,\phi,y) = \hat{y}\Phi^h_n(\phi)h^{ph}_{yj}(k_j^{ph},y) + \hat{\phi}\frac{1}{\xi_j^{ph^2}}\frac{\partial}{\rho\partial\phi}\Phi^h_n(\phi)\frac{\partial}{\partial y}h^{ph}_{yj}(k_j^{ph},y) \tag{A2}$$

$$\Phi^h_n(\phi) = \begin{cases}\cos(n\phi), & \text{PEC at } x=0\\ -\sin(n\phi), & \text{PMC at } x=0\end{cases} \tag{A3}$$

For TM_y mode:

$$\vec{e}^{pe}_{ctnj}(\rho,\phi,y) = \hat{y}\Phi^e_n(\phi)e^{pe}_{yj}(k_j^{pe},y) + \hat{\phi}\frac{1}{\xi_j^{pe2}}\frac{\partial}{\rho\partial\phi}\Phi^e_n(\phi)\frac{\partial}{\partial y}e^{pe}_{yj}(k_j^{pe},y) \tag{A4}$$

$$j\omega\mu\vec{h}^{pe}_{ctnj}(\rho,\phi,y) = \hat{\phi}\frac{k^2}{\xi_j^{pe2}}\Phi^e_n(\phi)e^{pe}_{yj}(k_j^{pe},y) \tag{A5}$$

$$\Phi^e_n(\phi) = \begin{cases}\sin(n\phi), & \text{PEC at } x=0\\ \cos(n\phi), & \text{PMC at } x=0\end{cases} \tag{A6}$$

where $e^{pe}_{yj}(k_j^{pe},y)$, $h^{ph}_{yj}(k_j^{ph},y)$ are eigenfunctions of the two parallel-plane waveguide. They can be solved using the method described in [7].

REFERENCES

[1] S. B. Cohn, "Microwave bandpass filters containing high-Q dielectric resonators," *IEEE Trans. Microwave Theory Tech.*, vol. MTT-16, pp. 218–227, Apr. 1968.

[2] W. H. Harrison, "A miniature high-Q bandpass filter employing dielectric resonators," *IEEE Trans. Microwave Theory Tech.*, vol. MTT-16, pp. 210–218, Apr. 1968.

[3] A. E. Atia and A. E. Williams, "Narrow-bandpass waveguide filters," *IEEE Trans. Microwave Theory Tech.*, vol. MTT-20, pp. 258–265, Apr. 1972.

[4] S. J. Fiedziuszko, "Dual mode dielectric resonator loaded cavity filter," *IEEE Trans. Microwave Theory Tech.*, vol. MTT-30, pp. 1311–1316, Sept. 1982.

[5] A. S. Omar and K. Schünemann, "Transmission matrix representation of finline discontinuities," *IEEE Trans. Microwave Theory Tech.*, vol. MTT-33, pp. 765–770, Sept. 1985.

[6] H. C. Chang and K. A. Zaki, "Evanescent-mode coupling of dual mode rectangular waveguide filters," *IEEE Trans. Microwave Theory Tech.*, vol. 39, pp. 1307–1312, Aug. 1991.

[7] S.-W. Chen and K. A. Zaki, "Dielectric ring resonators loaded in waveguide and on substrate," *IEEE Trans. Microwave Theory Tech.*, vol. 39, pp. 2069–2076, Dec. 1991.

[8] E. D. Nielsen, "Scattering by a cylindrical post of complex permittivity in a waveguide," *IEEE Trans. Microwave Theory Tech.*, vol. MTT-17, pp. 148–153, Mar. 1969.

[9] N. Okamoto, I. Nishioka, and Y. Nakanishi, "Scattering by a ferrimagnetic circular cylinder in a rectangular waveguide," *IEEE Trans. Microwave Theory Tech.*, vol. MTT-19, pp. 521–527, June 1971.

[10] C. M. Kudsia, R. Cameron, and W. C. Tang, "Innovations in microwave filters and multiplexing networks for communications satellite systems," *IEEE Trans. Microwave Theory Tech.*, vol. 40, pp. 1133–1149, June 1992.

[11] R. Gesche and N. Löchel, "Scattering by a lossy dielectric cylinder in a rectangular waveguide," *IEEE Trans. Microwave Theory Tech.*, vol. 36, pp. 137–144, Jan. 1988.

[12] X. P. Liang and K. A. Zaki, "Modeling of cylindrical dielectric resonators in rectangular waveguides and cavities," *IEEE Trans. Microwave Theory Tech.*, vol. 41, pp. 2174–2181, Dec. 1993.

[13] H.-W. Yao, K. A. Zaki, A. E. Atia, and R. Hershtig, "Full wave modeling of conducting posts in rectangular waveguides and its applications to slot coupled combline filters," *IEEE Trans. Microwave Theory Tech.*, vol. 43, pp. 2824–2830, Dec. 1995.

[14] K. A. Zaki, C. Wang, and A. E. Atia, "Dual mode conductor loaded cavity filters," in *26th European Microwave Conf.*, Prague, Czech Republic, Sept. 1996, pp. 159–162.

[15] C. Wang, K. A. Zaki, and A. E. Atia, "Dual mode conductor loaded cavity filters," *IEEE Trans. Microwave Theory Tech.*, vol. 45, pp. 1240–1246, Aug. 1997.

Chi Wang, for a photograph and biography, see this issue, p. 2392.

Hui-Wen Yao (S'92–M'95–SM'97) received the B.S. and M.S. degrees from Beijing Institute of Technology, Beijing, China, in 1983 and 1986, respectively, and the Ph.D degree from University of Maryland at College Park, in 1995, all in electrical engineering.

From 1986 to 1991, he was a Lecturer in the Department of Electrical Engineering, Beijing Institute of Technology, where his research dealt mainly with EM radiation, scattering, and antenna design. From 1991 to 1992, he held the position of Teaching Assistant in the Electrical Engineering Department, Wright State University, Dayton, OH, where he worked on microstrip circuits and transient scattering by cylinders. From 1992 to 1995, he was a Research Assistant in the Microwave Laboratory, Department of Electrical Engineering, University of Maryland at College Park, where he worked on analysis, modeling, and design of microwave and millimeter-wave devices and circuits. Since December 1995, he has been with the Space System Group, Orbital Sciences Corporation (formerly CTA Inc.), Germantown, MD, working on telecommunications and satellite communications.

Kawthar A. Zaki (SM'85–F'91), for a photograph and biography, see this issue, p. 2392.